

# Model Based Guiding Pattern Synthesis for on-Target and robust assembly of Via and Contact layers using DSA

Joydeep Mitra<sup>1</sup>, Andres Torres<sup>1</sup>, Yuansheng Ma<sup>1</sup>, and David Z Pan<sup>2</sup>

<sup>1</sup>Mentor Graphics Corporation

<sup>2</sup>University of Texas at Austin

## ABSTRACT

Directed Self Assembly (DSA) has emerged as one of the most compelling next generation patterning techniques for sub-7nm via or contact layers. A key issue in enabling DSA as a mainstream patterning technique is the generation of grapho-epitaxy based guiding pattern (GP) shapes to assemble the contact patterns on target with high fidelity and resolution. Current GP generation is mostly empirical, and limited to a very small number of via configurations. In this paper, we propose the first model-based GP synthesis algorithm and methodology for on-target and robust DSA, on general via pattern configurations. The final post-RET printed GPs derived from our original synthesized GPs are resilient to process variations and continue to maintain the same DSA fidelity in terms of placement error and target shape.

**Keywords:** Directed Self-Assembly (DSA), Multi-Patterning (MP), Guiding Pattern (GP), Compact Model

## 1. INTRODUCTION

DSA has been shown to be a compelling technology for printing the dense-pitched and low critical-dimension (CD) via/contact layer.<sup>2,6</sup> DSA can also be used in conjunction with existing multi-patterning (MP) techniques<sup>1</sup> to resolve coloring conflicts and reduce the cost of additional patterning masks and litho-etch steps. The self-assembly process for cylinder forming block copolymers is directed by guiding structures that utilize confinement (grapho-epitaxy, lithographically printed patterns) or surface affinity (chemo-epitaxy, chemically treated surfaces). The grapho-epitaxy process investigated here is compatible with traditional MP processes and is amenable to hybrid DSA-MP techniques.<sup>1</sup> The pitch multiplication property of DSA enables the printing of dense contact pitches below the resolvable lithographic pitch using the appropriate molecular composition of two block copolymers and by selecting the correct shapes for the grapho-epitaxy guiding patterns (GP). Since the chemical composition of the diblock copolymer is invariant in a specific DSA process, the accurate synthesis of GPs has now become the key bottleneck in the robust assembly of contacts to accurately match the placement of target contact shapes. The only existing work on the generation of GP shapes<sup>8</sup> is based on looking up a pre-characterized library of GP alphabet templates. It first maps groups of contacts into a list of discrete patterns and then selects from a list of pre-characterized GPs to encapsulate each contact group. This alphabet-based GP lookup methodology has the following drawbacks.

- Very regular 1-D standard cell layout patterns have been assumed in order to increase the probability of mapping contact patterns into the GP alphabet list. However, the majority of full custom cell layouts today still use 2-D styles with more complex via patterns at pin access regions of cells. Such complex and arbitrary via patterns make the discrete alphabet-based lookup schemes infeasible.
- The GP generation in<sup>8</sup> did not consider the effect of post-RET process variations, i.e., the post-RET image of the same alphabet may be different at various locations across the chip.

Figure 1 shows a sampling of contact pattern topologies that may occur in a typical 2D style layout designed using 7nm technology rules. In this small sampling we already see two contact groups that cannot be mapped into the finite alphabet set<sup>8</sup> due to relative pitch variations within the individual groups but were successfully synthesized using our model-based synthesis algorithm. The key objective of this paper is to develop a general framework for full-chip GP synthesis that directly addresses these drawbacks. Any method attempting to optimize the

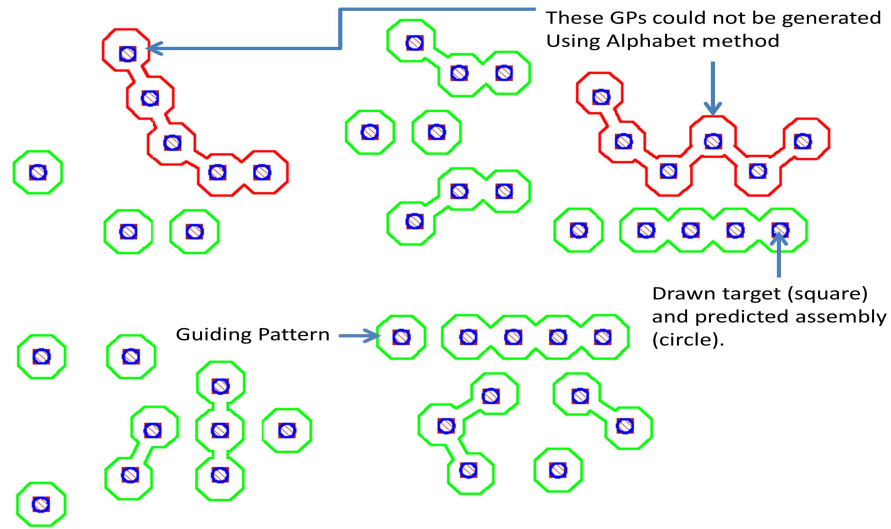


Figure 1. The two contact groups encompassed by the GPs in red could not be mapped into alphabet based GPs but were successfully synthesized using our methodology.

shape of a GP for accurate contact assembly needs to have the means to accurately predict the locations of assembled contact shapes given a GP as input. Since it is not practical to embed a full-physics DSA simulator directly into GP synthesis due to its prohibitive runtime, we need to ensure that our GP synthesis framework has the ability to plug-in any compact DSA model which is accurately calibrated against a full-physics based DSA simulator or experimental data with significantly faster runtime to enable full-chip simulations. In addition to accurately predicting assembly locations, any compact DSA model that has been integrated into our GP synthesis framework should also be able to evaluate the robustness of an input GP in regards to phase transition characteristics, in other words, there must be a metric to determine not only error placement but also how far a given guiding pattern is from experiencing phase transition, which in this case we define as not achieving the target cylinders.<sup>4</sup>

The key contributions of this paper are as follows:

- We propose the first model-based full-chip GP synthesis framework and optimization algorithm which targets two key objectives for on-target and robust DSA:
  - minimizing placement error (PE) between drawn target and assembled contact shapes;
  - minimizing the sensitivity of placement under guiding pattern variations induced by process fluctuations.
- We also describe an overall mask synthesis flow for DSA which includes DSA compliant contact grouping, GP synthesis, GP mask synthesis and RET, and finally a verification step that ensures the post-RET printed GPs will still assemble the contacts at the required locations and with the required shapes.
- We define the characteristics that a DSA compact model should have to satisfy the requirements of a GP synthesis framework. We illustrate the quality of results using a specific calibrated compact model.
- We define the metric of ‘Total Interaction Energy’ (TIE) that is used to characterize the robustness of a GP in regards to contact phase transformation and shape degradation. We find that with lower TIE the robustness of the GP improves.

The rest of this paper will be organized as follows. In Section 2 we will describe the overall DSA mask synthesis flow and compact model calibration methodology. In Section 3 we will formulate the GP synthesis

problem and constraints and describe our GP synthesis algorithm. In section 4 we will provide data based on the compact and Monte Carlo models demonstrating the robust assembly of arbitrary contact patterns by running detailed DSA simulations on our synthesized GPs. Section 4 will also provide an independent verification flow which will demonstrate that the post RET printed images of our synthesized GPs will still maintain compliance of assembled contact patterns. We will finally conclude in section 5.

## 2. DSA MASK SYNTHESIS FLOW

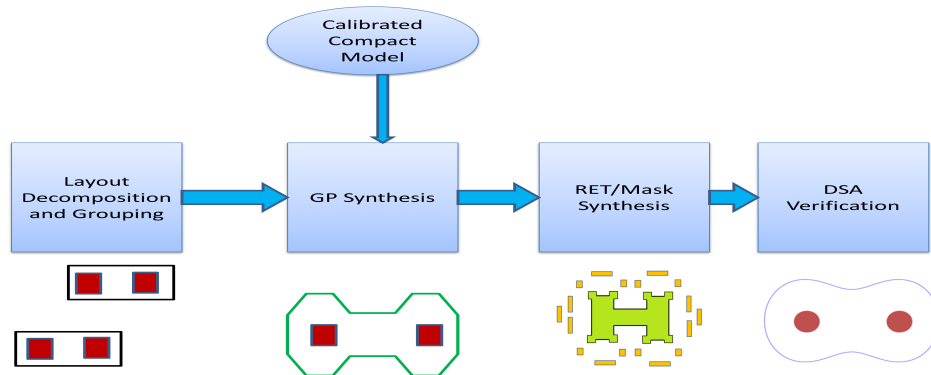


Figure 2. DSA mask synthesis and verification data flow.

### 2.1 The Overall Flow

Our mask synthesis data flow consists of four important subsystems as depicted in Figure 2. Given an input layout the first step is to partition the target contacts into DSA compliant groups. Each group is subject to the following constraints:

1.  $L_0 \leq d \leq d_{max}$  ( $d$  is the distance between adjacent contacts;  $L_0$  and  $d_{max}$  are the lower and upper bounds of contact pitches beyond which DSA-based assembly becomes unreliable).
2. Each DSA contact group needs to be at least  $L$  away from each other, where  $L$  is the minimum resolvable lithographic distance.
3. We only allow up to a maximum number of contacts (usually 4 or 5) per group, as above that number of cylinders, the assembly process becomes unreliable for most guiding patterns not centered at the natural period of the block copolymer.
4. In addition, 193nm immersion lithography requires the contact groups to be in horizontal/vertical formations whereas if EUV is used we may relax this constraint and allow angular orientations.
5. Finally, we only allow string formations and no branches due to unreliable assembly at the intersections in such formations. By this we mean that any contact may not have more than two neighbors at a distance  $d$  from it to be included in a unique DSA group.

Given successful contact layer partitioning into DSA compliant groups, the next step is to synthesize a GP for each group. Section 3 will explain our GP synthesis algorithm in detail. This is the key enabling step for DSA-based patterning and it is the main topic of this paper.

The next two steps involve RET of the synthesized GPs (such that the etched GP image is still within some tolerance of the target GP shape) followed by DSA simulation of the etched GP shape to verify that the assembled contacts still maintain fidelity toward the drawn targets with regards to contact placement and shape formation. Section 4 elaborates on these two steps.

## 2.2 Compact Model Calibration

As mentioned previously, in order for a GP synthesis algorithm to converge on a high quality GP with on-target and robust assembly, a compact model is needed that satisfies two key characteristics:

- fast prediction of contact assembly locations within an acceptable margin of error from a detailed DSA simulator.
- returns a metric which signifies robustness of the GP in regards to shape deformation and sensitivity to process variations.

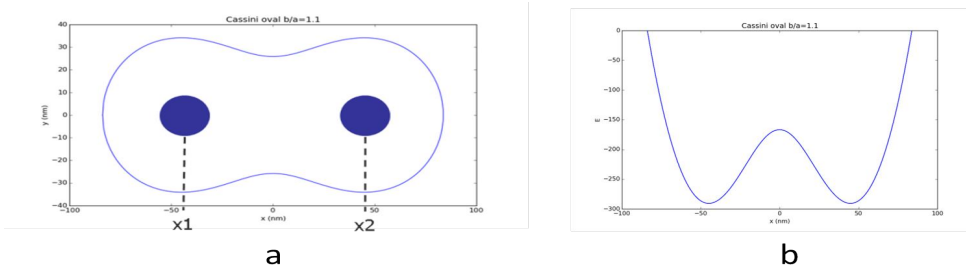


Figure 3. (a)Input GP to the simple compact model and predicted assembly locations  $x_1$  and  $x_2$ . (b)Total interaction energy of the system on the Y-axis as a function of X with two minimum energy solutions.

We will illustrate the key concepts using a simple compact model since the actual model used in this body of work is beyond the scope of this paper. Our compact model was calibrated to the detailed DSA simulation model described in<sup>3</sup> which involves minimizing the total interaction energy of the system. In the following example, our system consists of a single GP depicted by the Cassini Oval shape in figure 3(a). The total interaction energy is the Hamiltonian of potential and kinetic energy terms shown in equation 1 below:

$$\hat{H}(\vec{x}, \vec{v}) = P(\vec{x}) + K(\vec{x}, \vec{v}) \quad (1)$$

Assuming the system is quasi-static, the kinetic term may be neglected, hence:

$$\hat{H}(\vec{x}, \vec{v}) = P(\vec{x}) \quad (2)$$

Assume the cylinder interaction energy follows Hooke's law with stiffness coefficient  $k$  and intrinsic DSA period of  $L_0$ .

$$E_{selfassembly} = (k/2)(x_2 - x_1 - L_0) \quad (3)$$

The cylinders interact with the walls of the GP and we assume that the wall energy is a function of the guiding pattern width. Assuming a quadratic relationship:

$$E_{directed} = -((1 - k)/2)(y_{x_1}^2) - ((1 - k)/2)(y_{x_2}^2) \quad (4)$$

Hence, the total interaction energy of the system is given by:

$$E_{total} = E_{selfassembly}(L_0, k, x_1, x_2) + E_{directed}(k, x_1, x_2) \quad (5)$$

We define  $E_{total}$  specified in equation 5 as our metric TIE (Total Interaction Energy) which will help us select the most robust GP between competing GPs going forward. The locations of assembly  $x_1$  and  $x_2$  can then be found by minimizing the total energy of the system:

$$\begin{aligned} \min_{x_1, x_2}(E_{total}(L_0, k, x_1, x_2)) = \\ \min(-((1 - k)/2)(y_{x_1}^2) - ((1 - k)/2)(y_{x_2}^2) + k/2(x_2 - x_1 - L_0)) \end{aligned}$$

The model calibration suite of tools from<sup>7</sup> were then used to optimize compact model parameter values using a data set of GPs with known assembled contact locations. Our calibration results are shown in section 4.1.

### 3. GUIDING PATTERN SYNTHESIS

The DSA process itself consists of a litho-etch step to first pattern the GP trenches and then a spin-coating of the GP surface with a diblock copolymer consisting of two species usually Polystyrene(PS) and Polymethyl Methacrylate (PMMA) which we will refer to as A and B going forward. The molecular weight and volume fraction of the two species determines the phase segregation and cylindrical pattern formation upon thermal annealing. One of the two blocks is then selectively etched leaving the other block to act as a mask to be used as a contact pattern to be transferred onto the substrate.

#### 3.1 Synthesis Problem Formulation

In order to maintain fidelity towards the original contact CD, the GP will need to obey a volume fraction constraint which we will define as:

$$f = \text{volume}(A)/\text{volume}(A + B) \quad (6)$$

where  $A$  is assumed to be the block that forms the cylindrical contact pattern. In the context of a GP this constraint can be mapped into the following equation where  $\text{Area}(C(i))$  is the area of the  $i^{\text{th}}$  contact in a group of  $N$  within the GP contact group.

$$f = \sum_{i=1}^N \text{Area}(C(i))/\text{Area}(GP) \quad (7)$$

A GP then needs to meet the following two optimization objectives subject to the above constraint.

$$\text{Minimize}(\text{Maximum}(pe_i)) \quad (8)$$

$$\text{Minimize}(E_{total}) \quad (9)$$

where  $pe_i$  is the placement error (center to center displacement) between the drawn target contact and the assembled contact for the  $i^{\text{th}}$  contact in the group and  $E_{total}$  is the TIE of the GP. In the following two sections we first specify an algorithm that optimizes objective 8 above before simultaneously optimizing 8 and 9.

#### 3.2 Placement Error Minimization for On-Target Assembly

##### 3.2.1 Backbone Formation

Our solution begins with first creating a backbone which is defined as a shortest path that visits each contact exactly once. This backbone enables creating acceptable GP shapes which don't have cycles and branches. This problem is recognized as an application of the *Travelling Salesman Problem (TSP)*. Since our contact groups are strings due to the grouping constraints imposed in section 2, the TSP resolves to the simpler class of Euclidean TSP and can be solved in  $O(N(\log N))$  where  $N$  is again the number of contacts within the GP contact group under consideration.

##### 3.2.2 GP Shape Template Generation

We now need to form a seed shape that obeys constraint 7 from section 3.1 above. This seed shape will form a template for the final GP. This methodology needs to be able to recompute a new GP that meets the area constraint 7 whenever needed and will be used over and over in the Gradient Descent Algorithm described in section 3.2.3. Figure 4 below illustrates the seed shape and the backbone for a group of three contacts. The second seed on the right consists of four contacts indicating that contact groups may consist of arbitrary orientations as long as they follow the constraints listed in section 2.1. Figure 4 also indicates the parameters:

$T$  the initial sizing factor to grow the GP to meet the required area constraint 7.

$W_c$  the user specified connector width between octagons.

$W$  the contact width, assuming square contacts.

The seed GP shape generation is achieved using a thresholding mechanism to achieve the target GP area of constraint 7 which is equivalent to:

$$\text{Area}(GP) = (N * W^2)/f \quad (10)$$

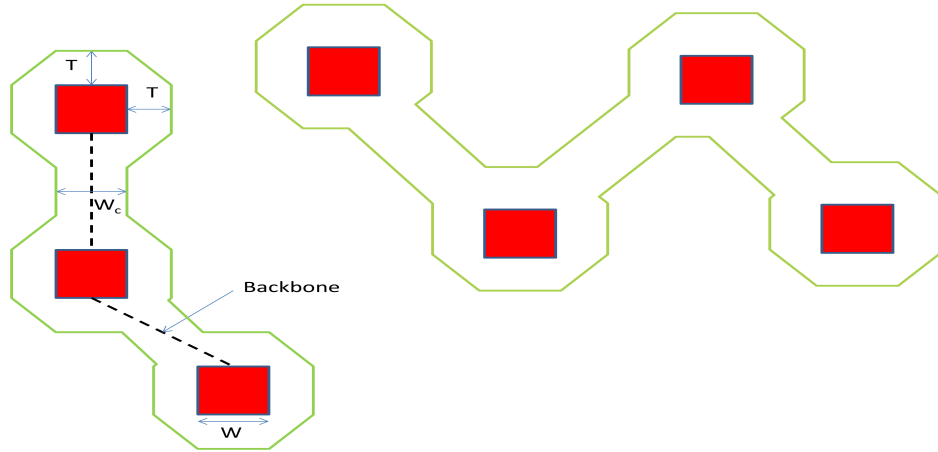


Figure 4. Two DSA compliant groups of three and four drawn target contacts encapsulated by an initial seed GP shape.

The initial sizing factor  $T$  is obtained by considering a single square contact of width  $W$ , chopping the corners by an amount  $C_l$  to form an octagon and then sizing the transformed contact up to obtain an octagonal GP of area  $A = W^2/f$ . This sizing factor is given by the equation:

$$T = (-b + \sqrt{b^2 - 4ac})/2a \quad (11)$$

where

$$\begin{aligned} a &= 4 \tan(\pi/8) \\ b &= 2W - C_l(1 - \tan(\pi/8)) \\ c &= 0.5(1 - 1/f)(W^2 - 2C_l^2) \end{aligned}$$

Starting with the sizing factor  $T$ , each transformed contact is then sized up or down together by small steps until the target area given by equation 10 above, of the merged shape including the sized contacts and the connectors of width  $W_c$ , is reached to a reasonable approximation. Algorithm 1 now becomes a building block which will be called later by the optimization kernel.

### 3.2.3 Gradient Descent PE optimization

Now that we have the building blocks from sections 3.2.1 and 3.2.2 we are ready to describe an algorithm that produces a solution that minimizes PE. Let us represent the original target contact locations by the vector  $S^*$  consisting of a set of  $N$  points corresponding to the centers of the drawn targets. We now use the following gradient descent formulation where the next solution vector  $S'$  is given by:

$$S' = S - \gamma(P - S^*) \quad (12)$$

Where  $S$  is the current solution,  $\gamma$  is a learning feedback factor and  $P$  is the vector of contact locations predicted by the compact model for the current GP generated from  $S$ . The intuition behind the above formulation is that the term  $(P - S^*)$  determines the direction in which the current solution must move in order to converge on the ideal locations  $S^*$ . The trajectory of a specific GP convergence is depicted in figure 5. We iterate equation 12 until we have converged on a solution vector within an acceptable margin of error. An algorithm to generate a GP that minimizes the PE between the assembled and drawn target contacts is specified in Algorithm 2. The input to this algorithm is a set of target contact locations and the output is an encapsulating GP that minimizes PE.

---

**Algorithm 1:** generate GP shape

---

**input** : Vector of transformed target contact shapes  $S$   
**output:** GP shape that satisfies equation 7

- 1  $A$  = Target area from equation 10;
- 2  $T$  = initial sizing factor from equation 11 above;
- 3  $C$  = list of  $N - 1$  trapezoidal connectors between  $N$  contacts in  $S$ ;
- 4  $A'$  = area of GP shape computed from  $(S, C)$  by sizing  $S$  by  $T$ ;
- 5  $step$  = small step size by which  $T$  is modified below;
- 6 **if**  $A' \leq A$  **then**
- 7    $dir = +1$
- 8 **else**
- 9    $dir = -1$
- 10 **while**  $|A - A'| \leq \epsilon$  **do**
- 11    $T = T + dir * step$ ;
- 12    $A'$  = area of GP shape computed from  $(S, C)$  by sizing  $S$  by  $T$ ;

---

---

**Algorithm 2:** minimize PE kernel

---

**input** : Vector of target contact locations  $S^*$ , Compact Model (CM)  
**output:** Optimized GP

- 1  $B$  = generate Backbone by solving TSP;
- 2  $S = S' = S^*$ ;
- 3  $GP(S)$  = generate initial GP shape using algorithm 1;
- 4  $P(S)$  = CM predicted contact locations using  $GP(S)$ ;
- 5 **while**  $|P(S') - S^*| \geq \epsilon$  **do**
- 6   **if**  $|P(S') - S^*| > |P(S) - S^*|$  **then**
- 7      $break$  out of loop since we have diverged
- 8   **else**
- 9      $S = S'$ ;
- 10      $S' = S - \gamma(P(S) - S^*)$ ;
- 11      $GP(S')$  = generate GP shape using algorithm 1;
- 12      $P(S')$  = CM predicted contact locations using  $GP(S')$ ;

---

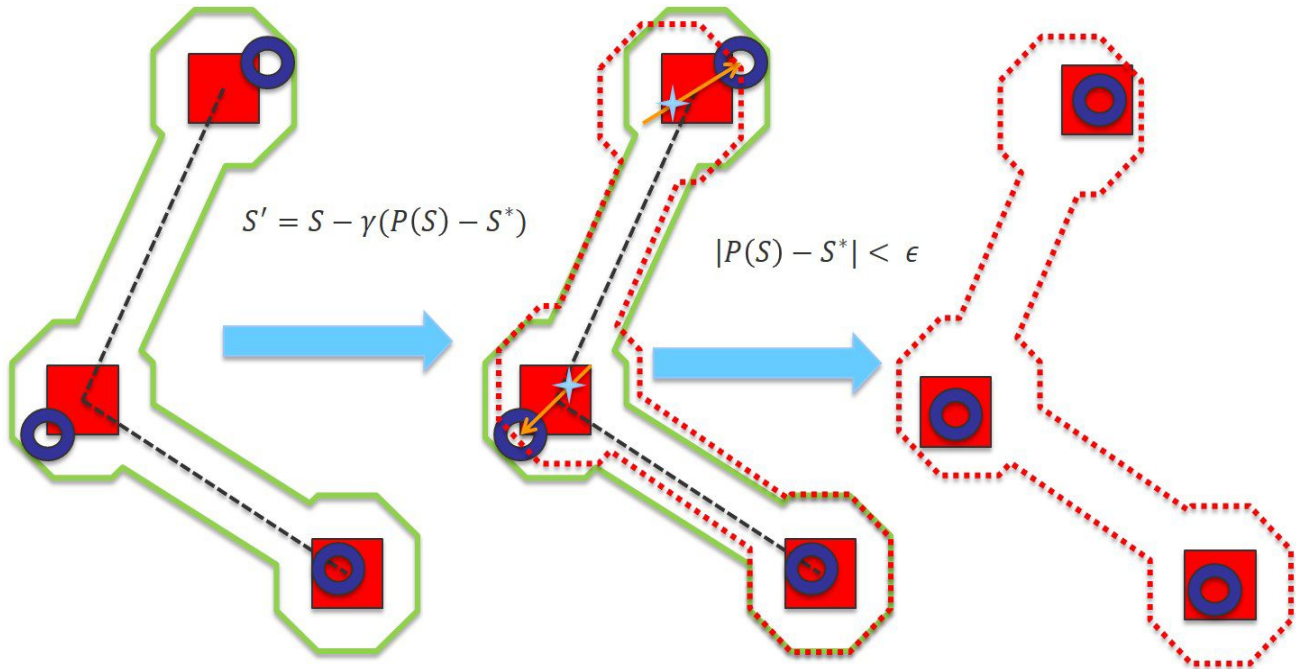


Figure 5. Gradient Descent placement error optimization algorithm converging on a GP that minimizes PE.

### 3.3 Energy Minimization for Robust assembly

We have up to this point shown a method to synthesize GPs that consider only PE as an optimization objective. Unfortunately for robust assembly optimization of this metric alone is not enough. The GP needs to also be able to assemble contacts that are not in phase transition. GPs defining targets which would require a higher than normal equilibrium energy are deemed to be in phase transition. Figure 6 suggests that there is a direct correlation between TIE and robust assembly. Each data point in the scatter plot is a GP shape ordered by increasing TIE in the X-axis and increasing probability of failure in the Y-axis. Probability of failure was measured by running 30 Monte-Carlo simulations for each GP and measuring the shape deviation in three dimensions from the ideal cylindrical shape for each target contact in each simulation. If a failure was encountered in every run for a GP then the probability of failure was 1 and if there was no failure in any of the runs then the GP was considered robust with a probability of failure of zero. Each GP was expected to assemble exactly two contacts. In the figure, the GP with the highest TIE on the extreme right is assembling a third contact at the center instead of the two required contacts. Hence, we now have the motivation for using TIE as a second metric for generating robust GPs. We will also show in section 4 that such GPs are resilient to post-OPC process variations as well.

Now that we have a kernel to generate a GP optimized for PE we will enumerate a method that simultaneously optimizes both PE and TIE. Prior work<sup>5</sup> on the TEEF metric has shown that the robustness of assembly is most sensitive to the  $CD_{TY}$  and  $CD_{TBW}$  parameters in the TEEF matrix. These parameters and others used in TEEF are shown in Figure 7. As described in sections 3.2.2 and 3.2.3, our seed GP shapes are obtained by transforming the original contacts through a series of corner rounding and sizing operations, and then merging the transformed shapes with fixed width connectors along the backbone while maintaining constraint 7. Since it is the contact that forms the seed for the final GP shape, we can further transform the seed contact to now enable us to sweep through various aspect ratios of the octagonal sections while still maintaining constraint 7. The changing aspect ratios enable us to sweep through the TEEF parameter  $CD_{TY}$ . In addition, the other TEEF sensitive parameter  $CD_{TBW}$  directly maps onto our connector width parameter  $W_c$ . We can now incrementally sweep through various contact aspect ratios and connector widths and continue to use algorithm 2 to minimize the PE for each GP shape configuration and choose the configuration with minimum TIE returned from our compact model. Figure 8 depicts the GP shape transformations for finding a GP with TIE while maintaining

constraint 7 for each intermediate GP shape.

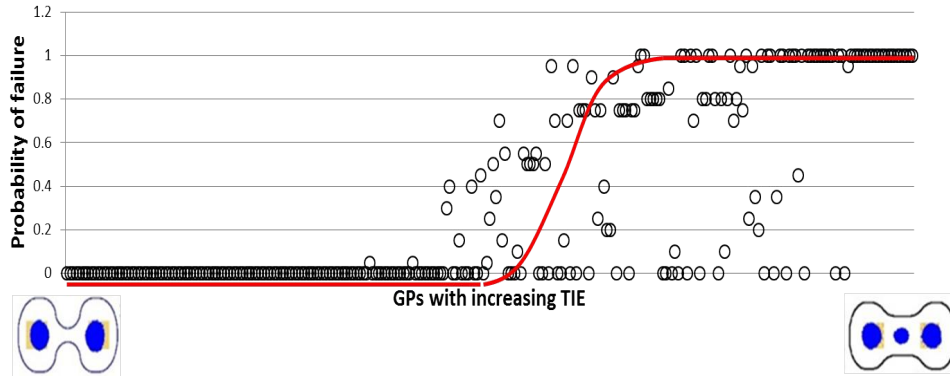


Figure 6. As the GP TIE increases, the probability of failure and phase transition increases as well.

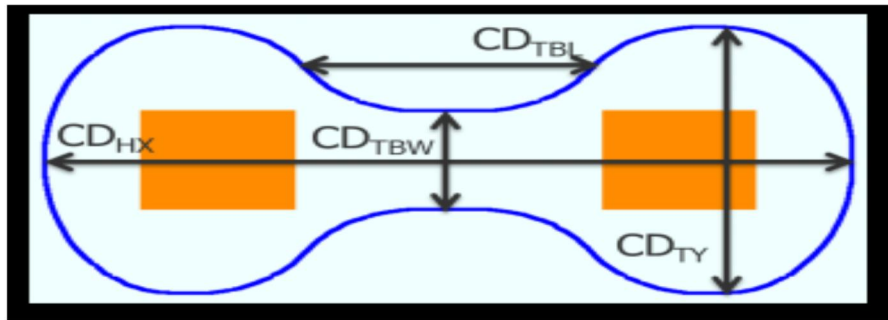


Figure 7. GP template and various TEEF parameters for a doublet pattern.

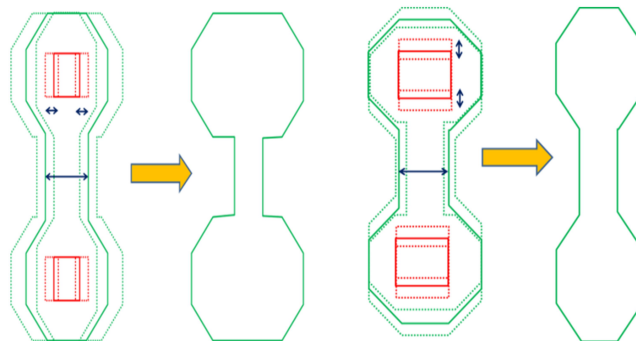


Figure 8. Varying seed contact aspect ratios and connector widths to obtain GP with minimum energy.

Algorithm 3 shows our overall methodology for simultaneous optimization for both PE and energy. It has an outer loop that sweeps through incrementally varying connector widths and an inner loop which sweeps through incrementally varying contact aspect ratios creating virtual contact seeds for the resulting GP shapes while still maintaining the area fraction constraint 7 corresponding to the original square contacts. It shall be noted that we could have exited the above loops at inflection points but our experience has been that the correlation function between TEEF and energy does not have a single extremal point but our objective is to find the global minimum

---

**Algorithm 3:** minimize GP energy

---

**input** : Vector of initial target contact locations  $S^*$ , Compact Model (CM)  
**output**: Optimized GP

- 1  $C_W$  = Default connector width;
- 2  $C_B$  = User supplied bound for  $C_W$  exploration;
- 3  $W_B$  = User supplied bound for aspect ratio exploration;
- 4  $optGP$  = initialize with a default GP;
- 5  $minEnergy$  = initialize with large number;
- 6 **for**  $C_W$  *in*  $[C_W - C_B, C_W + C_B]$  **do**
- 7      $W'$  = original contact width;
- 8     **for**  $W' \geq W_B$  **do**
- 9          $W' = W' - step$ ;
- 10          $S_X^*$  = vector of new contacts with horizontal width modified to  $W'$ ;
- 11          $S_Y^*$  = vector of new contacts with vertical width modified to  $W'$ ;
- 12          $(minEnergy_x, GP_X)$  = use algorithm 2 with input  $(S_X^*, C_W)$ ;
- 13          $(minEnergy_y, GP_Y)$  = use algorithm 2 with input  $(S_Y^*, C_W)$ ;
- 14          $minEnergy = minimum(minEnergy, minEnergy_x, minEnergy_y)$ ;
- 15          $optGP = GP$  corresponding to  $minEnergy$ ;

---

and hence the exhaustive search. In practice Algorithm 3 can be provided with a starting exploration point from which to begin the search based on regression analysis of prior data.

## 4. EXPERIMENTAL RESULTS

### 4.1 Compact Model Calibration

As described earlier in section 2.2 the compact model was calibrated to Monte Carlo simulations produced following the theory developed by.<sup>3</sup> Figure 9 shows the result of the calibration process. It shows the minimum error that can be achieved for a specific period  $L_0$  of the block copolymer. This signature has been previously observed in compact models capable of predicting phase transition by defining the maximum energy at which proper assembly takes place.<sup>4</sup> Figure 9 shows that for an  $L_0$  range between 33nm and 50nm the calibration error was under 2nm where calibration error is the average of PE and shape deformation from the ideal cylindrical shape.

### 4.2 GP Synthesis

We first validated our PE minimization kernel on 8 industry benchmark circuits. We calibrated compact models matching Monte Carlo Simulations and applied it to each of the benchmarks since some of the benchmarks were based on different technology processes. For some of the benchmarks even though there were mismatches between the DSA natural period ( $L_0$ ) parameter described in sections 2 and 2.2 due to pitch variations of the benchmarks between 35nm and 65nm, our synthesizer still converged on GP shapes which achieved robust assembly. We first partitioned each circuit into DSA compliant groups as described in Section 2. We then extracted the set of unique DSA compliant contact pattern groups for each circuit. Our framework uses a variant of the *TRIE* prefix lookup data structure to only synthesize unique topologies thus significantly saving runtime. We then ran our synthesizer through each circuit and mostly observed 100% synthesis of each set of the unique groups. The one circuit which showed a few failures was due to extreme acute angle orientations between adjacent contacts. Our algorithm selects the GP shape that simultaneously minimizes both PE and TIE. We instrumented our code to output samplings of high energy GPs for every unique contact topology in our 8 benchmarks and then sized each GP up and down by 2nm to emulate process variations. We then performed detailed DSA simulation on each of these GPs. One set of GPs had a contact spacing of 40nm which was close to the  $L_0$  value of 35nm for this process. The other set of GPs had a contact spacing of 50nm. Detailed Monte-Carlo DSA simulation showed

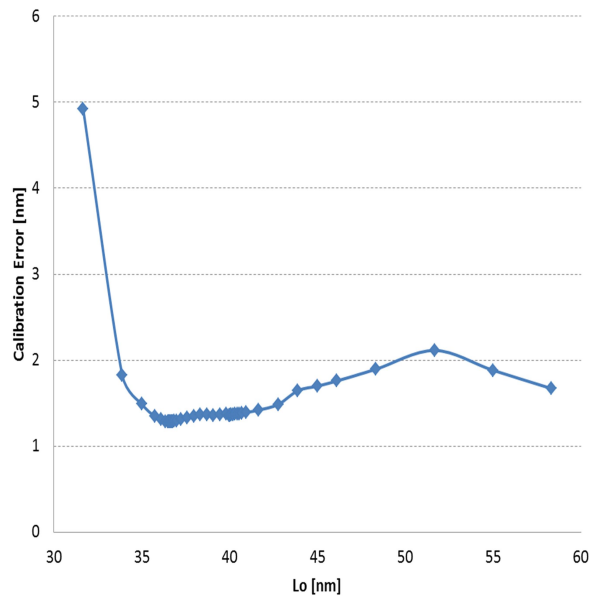


Figure 9. Calibration error as a function of the natural period model parameter ( $L_0$ ) of the diblock copolymer.

that shape displacement is on the order of 9nm for high energy GPs as opposed to negligible displacement for low energy GPs as shown on Figure 10A thus demonstrating the importance of our TIE metric used for GP synthesis. Figure 10B shows that the high energy GP is far more sensitive to process variations with a PE range of almost twice (13nm) that of the low energy GP (7nm).

### 4.3 Mask Synthesis of GP and Verification

One of the main goals of improving robustness of the assembly process to GP variations is due to the process variations during the lithographic process. Figure 11A shows the target holes within the synthesized groups considering the optimal (low energy) GP, and a large energy solution for the same target pitch. Notice how in this decoupled flow, the final nominal contour deviates from the ideal GP, raising the importance of generating a GP that is more robust to fluctuations in its shape with respect to the assembly process.

The actual holes after assembly resulting from the GP produced by a 193nm immersion process are shown in Figure 11B. After introducing 40nm defocus and +/- 2% dose variation, the GPs produce very different error placement results. While the average GP variation for most of the patterns is within a 2nm range, even 4nm range differences in the GP are able to be absorbed by the low-energy GP configuration. In contrast, the GP with higher nominal energy shows indeed a higher sensitivity in error placement due to the GP variation. Error placement was only computed when the model returned a valid configuration. Notice how the guiding pattern obtained by considering the approach proposed in this work, delivers a smaller error placement for the same process variations.

## 5. CONCLUSIONS

This paper proposes a model-based GP synthesis algorithm with a focus on accurate placement, robust shape fidelity and resiliency to post-RET process variations. To our knowledge this is the first body of work that simultaneously achieves all these milestones. We first introduced a DSA-centric mask synthesis flow which included a post-RET verification step of our GPs that maintained accurate placement and robust shape formation resiliency through process variations. We then proposed a model based GP synthesis algorithm that uses a

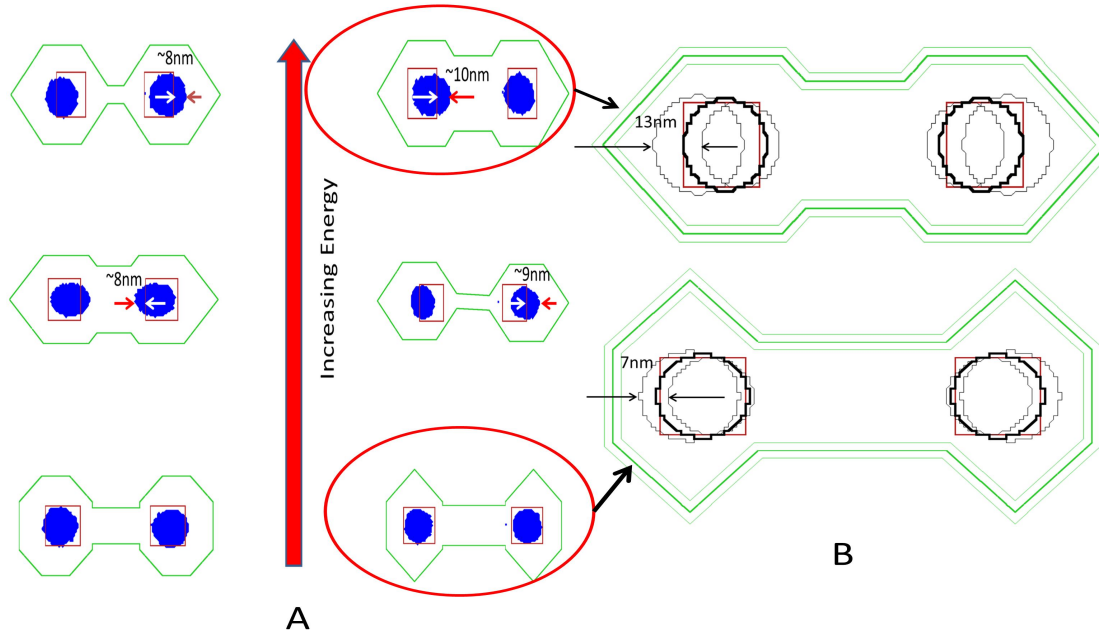


Figure 10. (A) The left GPs have contact spacing of 40nm and the ones on the right have 50nm. The bottom GPs have minimum energy. We see phase transition and shape distortion begin to happen as the GP energy increases. (B) The high energy GP shows almost twice the sensitivity to process variation than the low energy GP.

compact model to predict the next solution in a gradient-descent based approach. Our synthesis algorithm also included GP shape exploration to search for both a minimum energy and minimum PE shape configuration. We then provided the quality of results for a specific compact model calibrated for a specific process along with correlation of internal GP energy to the TEEF metric which provides a measure of robustness of assembly. This work provides an avenue to understand the observed experimental displacement error reported by most research groups, and it provides an avenue to reduce it by finding the guiding pattern solution with minimum TEEF.

## REFERENCES

1. Y. Badr, A. Torres, and P. Gupta. Mask assignment and synthesis of DSA-MP hybrid lithography for sub-7nm contacts/vias. In *Design Automation Conference, 2015*, 2015.
2. X.-Y. Bao, H. Yi, C. Bencher, L.-W. Chang, H. Dai, Y. Chen, P.-T. Chen, and H.-S. Wong. Sram, nand, dram contact hole patterning using block copolymer directed self-assembly guided by small topographical templates. In *Electron Devices Meeting (IEDM), IEEE International, 2011*, 2011.
3. F. A. Detcheverry, H. Kang, K. C. Daoulas, M. Muller, P. F. Nealey, and J. J. de Pablo. Monte carlo simulations of a coarse grain model for block copolymers and nanocomposites. *Macromolecules*, 41(13):4909–5001.
4. G. Fenger, A. Burbine, J. A. Torres, Y. Ma, Y. Granik, P. Krasnova, G. Vandenberghe, R. Gronheid, and J. Bekaert. Calibration and application of a dsa compact model for graphoepitaxy hole processes using contour-based metrology. In *Proc. SPIE 9235, Photomask Technology 2014, 92351X (8 October 2014)*.
5. Y. Ma, J. Lei, J. Torres, L. Hong, J. Word, G. Fenger, A. Trichtkov, G. Lippincott, R. Gupta, N. Lafferty, Y. He, J. Bekaert, and G. Vanderberghe. Directed self-assembly (dsa) grapho-epitaxy template generation with immersion lithography. In *Proc. SPIE 9423, Alternative Lithographic Technologies VII, 942306(2015)*, 2015.
6. Y. Ma, J. Torres, G. Fenger, Y. Granik, J. Ryckaert, G. Vanderberghe, J. Bekaert, and J. Word. Challenges and opportunities in applying grapho-epitaxy dsa lithography to metal cut and contact/via applications.

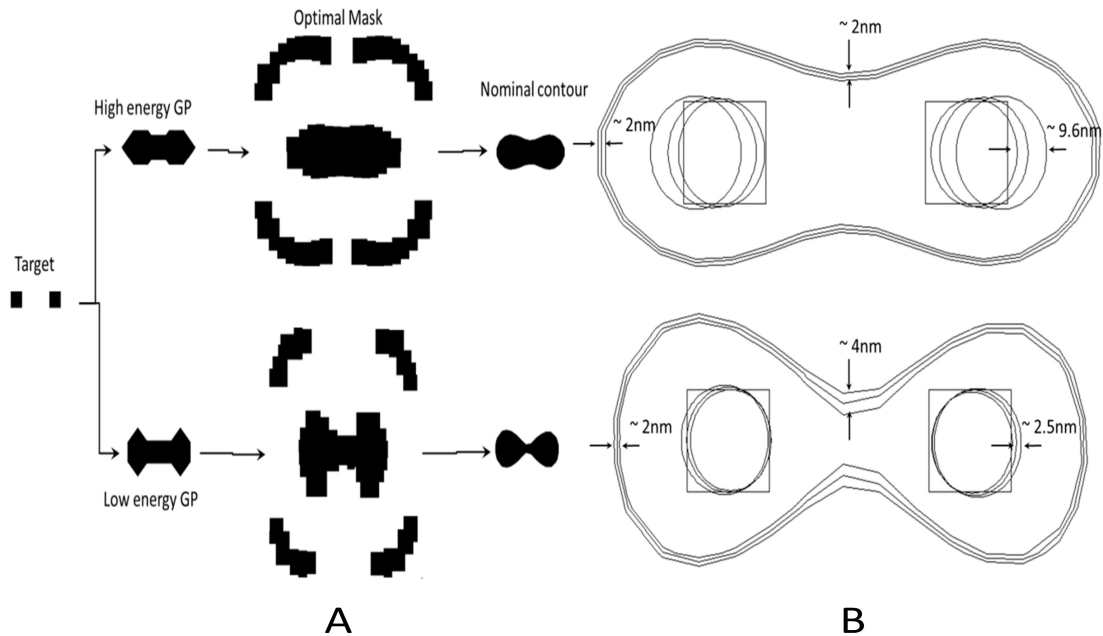


Figure 11. (A) Target GP generation (low and high energy GP, optimal mask and contours at nominal condition). (B) Top shows the GP for a higher energy GP, while the lower figure shows the GP for a minimum energy GP.

In *30th European Mask and Lithography Conference, International Society for Optics and Photonics, 2014*, 2014.

7. Mentor Graphics Corp. *Calibre Workbench suite of tools*.

8. H. Yi, X.-Y. Bao, R. Tiberio, and H.-S. P. Wong. A general design strategy for block copolymer directed self-assembly patterning of integrated circuits contact holes using an alphabet approach. *Nano Letters*, 15(2), 2015.